Proceedings of ASME IMECE2008
International Mechanical Engineering Congress & Exposition
October 31- November 6, 2008, Boston, Massachusetts, USA

IMECE2008-68110

Stress Analysis of Hygrothermal Delamination of Quad Flat No-lead (QFN) Packages

Minshu Zhang[1], S. W. Ricky Lee[1], Xuejun Fan[2]
[1]Department of Mechanical Engineering
Hong Kong University of Science and Technology
Clear Water Bay, Kowloon, Hong Kong
[2]Department of Mechanical Engineering
Lamar University
Beaumont, Texas, USA

ABSTRACT

Interfacial delamination is the major reliability issue of Quad Flat No-lead (QFN) packages under the JEDEC-MSL preconditioning and reflow process. Failures will occur when the hygrothermal stress exceeds the interfacial strength. Simulation based on finite element model is a popular method for studying the failure mechanism. However, the non-accurate material properties and lack of experiment validations always constrain the Finite Element Analysis (FEA) at the artificial parametric study stage.

To further investigate the interfacial delamination, a complex system both including simulation and experiment validation is established in this study. A dummy QFN is fabricated first as the test vehicle for subsequent study. Then the related finite element model is also built up to reveal the interfacial stress distribution when the packages are subjected to the pure thermal loading and hygrothermal loading. Once the interfacial stress is derived, the strength approach is applied here to indicate the high risk area where delamination will occur. Finally, the analyses from simulation are verified by Moisture Sensitivity Level (MSL) tests using dummy samples.

In this paper, a superposition method is used to integrate the thermo-mechanical and hygro-mechanical stress together, considering the non-uniform moisture distribution during reflow. The shear stress is found to be dominated along all the interfaces. From the comparison between simulation and experiments, the strength approach is applied to evaluate the package reliability successfully. Both simulation and experiment results show that the molding compound/lead-frame interface around the junction of die attach fillet would be the initiation of delamination.

INTRODUCTION

Quad Flat No-lead (QFN) package known as one of the Surface Mount Technology Device (SMTD) is widely used in industry. The major features are low cost, low pin-count requirement and high thermal dissipation. In particular, there is one critical challenge in SMT applications which is interfacial delamination during reflow. This failure could be observed in Quad Flat Packages (QFP), Thin Array Plastic Package (TAPP), Flat Bump Package (FBP) and other lead-frame based packages.

The reasons for interfacial delamination could be traced to thermal mismatch effect, moisture absorption and degradation of interfacial adhesion. Simulation based on finite element model is a popular method to study the failure mechanism. Tee and Zhong **[1]** established an integrated stress model in order to consider all the effects together. The thermo-mechanical, hygro-mechanical and vapor stress were calculated separately with lots of modeling techniques then integrated into one model. However, the failure mechanism is still not clear since the critical interfacial stress was not discussed and the simulation result lacks experiment validation. Driel et al **[2]** also discussed the initiation of delamination in QFN using interfacial fracture mechanics. But the simulation result was really dependent on the location and the length of the pre-crack. Therefore, the contribution to the failure of each effect needs to be identified with more experiment validations.

To break the gap between FEA and experiment validations, a complex system shown in Figure 1 is established to study the failure mechanism of hygrothermal delamination. Two kinds of dummy QFN packages with different lead-frame will be manufactured as the test vehicles for this study. The research methodology generally divides into two routes. One follows the simulation route, starting from material characterization to finite element modeling. Strength approach is then applied to evaluate the package reliability. In the other route, dummy QFN are fabricated and tested to provide experiment result for later comparison. The stress analysis with red background will be discussed in this paper, more details about the sample preparation and experiment tests with yellow background is introduced in reference **[3]**. The major objectives of this paper are given as follows:

- A finite element model will be established to figure out the interfacial stress distribution along different interfaces when dummy QFN is subjected to the pure thermal loading and hygrothermal loading.

- Strength approach is applied to evaluate the package reliability and indicate the high risk area where delamination will occur. Complete experiment validation will be carried out to verify the validity of the strength approach.

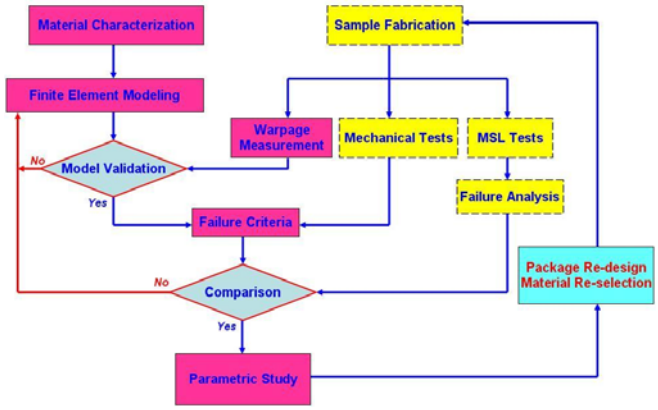

Figure 1. Research Methodology

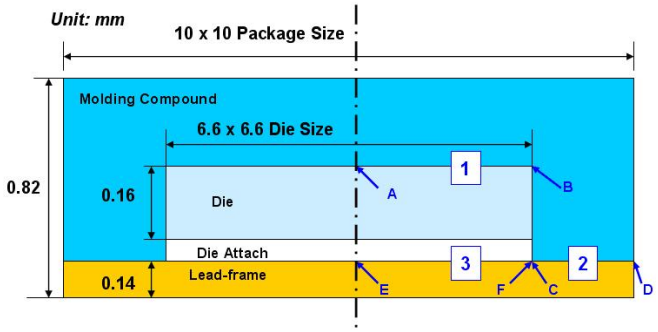

Figure 2. Schematic of Dummy QFN Package

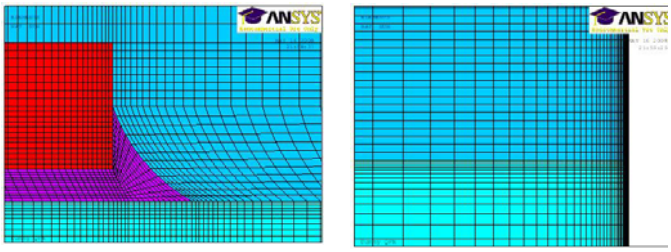

(a) FEM mesh at die attach fillet (b) FEM mesh at package edge

Figure 3. 2-D Half Model for Dummy QFN Package

FINITE ELEMENT MODEL

Dummy QFN package generally includes four major parts: lead-frame, die attach, die and molding compound. The dimensions and configurations are shown in Figure 2. Two kinds of dummy QFN will be studied in this paper. The one with silver lead-frames is noted package 1. The other, with PPF lead-frames, is noted package 2.

A 2-D half finite element mode is established using ANSYS code including 8744 4-nodes quad-elements. A finite element mesh is shown in Figure 3. The finer mesh is given at the junction of die attach fillet and the package edge. The mesh density around the package edge is very high in order to match the free edge effect. The same model will be used for subsequent different analysis only changing the element types and material properties.

THERMO-MECHANICAL STRESS ANALYSIS

In order to clarify the contribution of pure thermal effect, it is first necessary to understand the temperature distribution. The governing equation of transient heat transfer could be described as follows:

$$\frac{\partial T}{\partial t} = \alpha_T \left(\frac{\partial^2 T}{\partial x^2} + \frac{\partial^2 T}{\partial y^2} + \frac{\partial^2 T}{\partial z^2} \right) \quad (1)$$

where T is the temperature, x, y, z, are the spatial coordinates, and α_T is the thermal diffusivity. The boundary condition applied here is fixing of the external surface temperature according to the reflow profile (Pb-free) shown in Figure 4. The thermal material properties specific heat (C_p), thermal conductivity (k), and density (ρ) are listed in Table 1.

Table 1. Material Properties for Thermal Analysis

Material	C_p (J/kg ^{o}K)	k (W/m ^{o}K)	ρ (kg/m^3)
Lead-frame	385	385	8960
Die (Si)	750	124	2329
MC	2021	1.26	1280
DA	600	4	2000

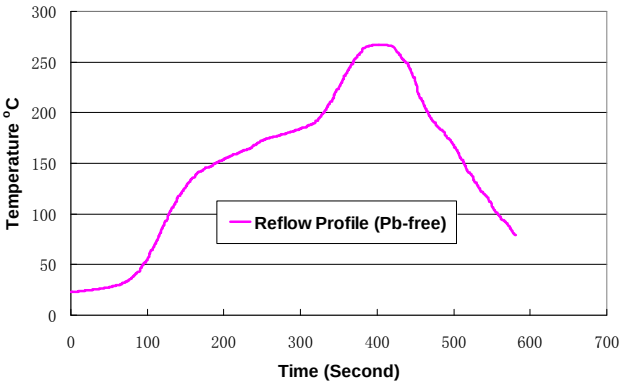

Figure 4. Reflow Profile

However, the heat was conducted very fast due to the high conductivity of copper and die (Si). The internal package achieved quite uniform temperature at different sections. When the package was heated up to peak temperature at 260^{o}C, the temperature gradient was no more than 1 ^{o}C. Therefore, the temperature distribution during reflow could be assumed to be uniform throughout the package in the subsequent thermo-mechanical analysis.

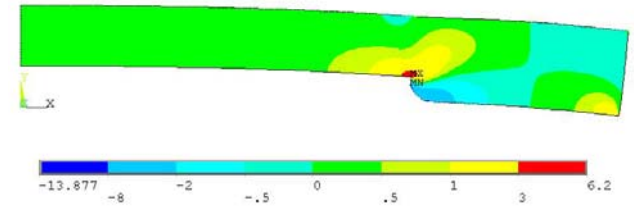

(a) Shear stress acting in molding compound

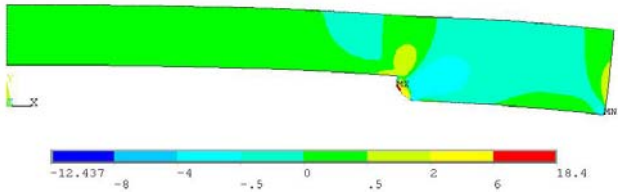

(b) Peeling stress acting in molding compound

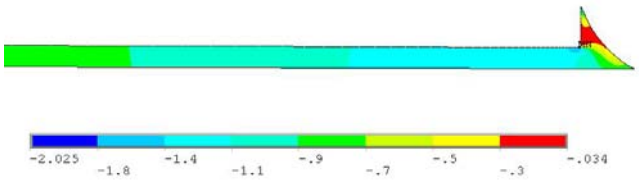

(c) Shear stress acting in die attach

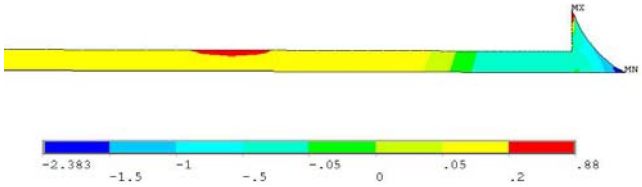

(d) Peeling stress acting in die attach

Figure 5. Thermo-mechanical Stress Distribution at 260°C

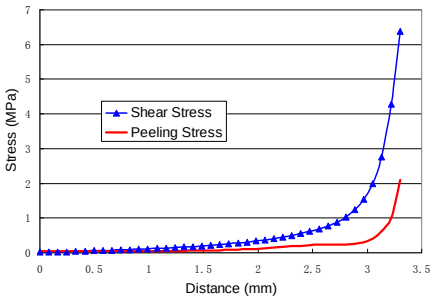

(a) Path 1, A-B

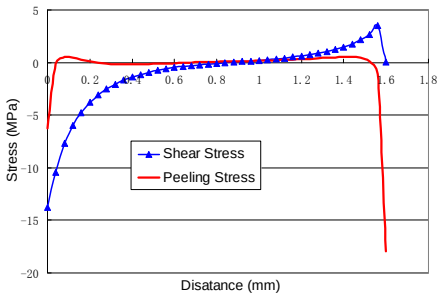

(b) Path 2, C-D

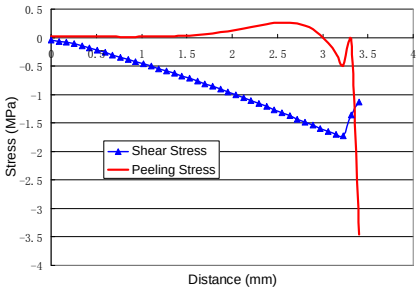

(c) Path 3, E-F

Figure 6. Interfacial Stress Distribution from Thermo-mechanical Stress Analysis at 260°C

Table 2. Material Properties for Thermo-mechanical Stress Analysis

Material	*E (GPa)*	*v*	α (ppm/°C)
Lead-frame	80	0.34	18
Die (Si)	110	0.28	4
MC	1.10	0.30	55.7
DA	0.04	0.30	151

For the thermo-mechanical modeling, the temperature was raised from 175°C (Curing temperature) to 260°C (Peak temperature for Pb-free reflow). Linear-elastic material properties were applied here seen in Table 2.

$$\varepsilon_T = \alpha \Delta T \quad (2)$$

Applying Eq. (2), the thermo-mechanical stress was derived shown in Figure 5. Since the major concern was at the interface, only shear stress and peeling stress were plotted. To be noticed here, the commercial code will average the stress values at the interface between elements. This would be correct only if the structure is made of one kind of material **[4]**. When the interface crosses over two different materials, it will lead to the wrong results. The procedure to obtain the correct interfacial stress distribution is to select all the elements with the same material then output the nodal stress results at the related interface.

The interfacial stress distributions at different interface were shown in Figure 6 and the paths were defined in Figure 2. Path 1 was at the die top surface from the die center (Point A) to the die edge (Point B). In path 1, interfacial shear stress was dominated and the maximum value achieved to 6.38 MPa at point B. Path 2 was at the molding compound/lead-frame interface starting from the junction of die attach fillet (Point C) to the package edge (Point D). In path 2, shear stress was dominated again since the peeling stress was all minus value which meant the peeling stress contribute to the compression effect to the interface and would not induce the delamination. The shear stress concentrated at point C and point D about 13.82 MPa and 3.45 MPa respectively. Path 3 was at the die attach/lead-frame interface starting from die center (Point E) to the edge of die attach region (Point F). Similar as other two

paths, shear stress remained the dominant stress component with maximum value at point F about -1.7 MPa. Once the interfacial stress distributions were derived, the failure criterion can be described as follows:

$$D = [\frac{\tau}{S}] \tag{3}$$

where τ means the shear stress from FEA calculation, S means the interfacial shear strength from mechanical tests seen in Table 3, D means the failure factors. The larger the value of D, the higher the possibility of failure. In this study, button shear and die shear tests were conducted to determined the interfacial shear strength. More details are presented in reference **[3]**. From the calculations of D listed in Table 4, some estimation could be given as follows:

- Compare the D in rows, point C has the highest value among all which means the delamination will initiate at molding compound/lead-frame interface around the junction of die attach fillet.
- Compare the D in columns, the values at point C in package 2 are higher than the ones in package 1 which means package 2 will have lower reliability against the interfacial delamination than package 1.

Table 3. Interfacial Shear Strength (MPa)

MC/Si	MC/ LF_{Ag}	MC/ LF_{PPF}	DA/ LF_{Ag}	DA/ LF_{PPF}
10.00	11.23	7.56	7.55	27.33

Table 4. Calculation of Failure Criterion Factors D

	1) MC/Si (A-B)		2) MC/LF (C-D)		3) DA/LF (E-F)	
	A	B	C	D	E	F
Maxi Shear Stress (MPa)	0	6.38	-13.82	-3.45	0	-1.70
Maxi Peeling Stress (MPa)	0	2.01	-6.23	-17.91	0	-3.50
D_{Ag}=[τ/S]	0	0.64	**1.23**	0.31	0	0.22
D_{PPF}=[τ/S]	0	0.64	**1.83**	0.46	0	0.06

With the above expectations, the experiment validations were implemented following the test A in Figure 7. In order to apply the pure thermal effect to the packages, the dummy QFN went through reflow just after 24 hours baking without moisture preconditioning. Then the C-SAM inspections showed that package 1 could pass test A seen in Figure 8 when package 2 totally failed at this stage seen in Figure 9. From the C-Scan images in Figure 9, most of the outside boundaries of the delamination area (red area) pointing to the package edge were smaller than the inside ones. Combined with the delamination propagation trend we may conclude that delamination initiated at the molding compound/lead-frame interface around the junction of die attach fillet. The T-Scan images also reflected the C-Scan observations and confirmed the safety of die attach region beneath the die.

Figure 7. Flow Chart of Experiments using Dummy QFN

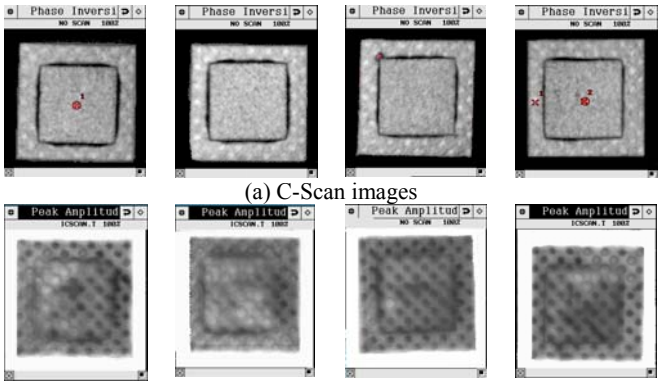

(a) C-Scan images

(b) T-Scan images

Figure 8. C-SAM Inspection of Package 1 after Test A

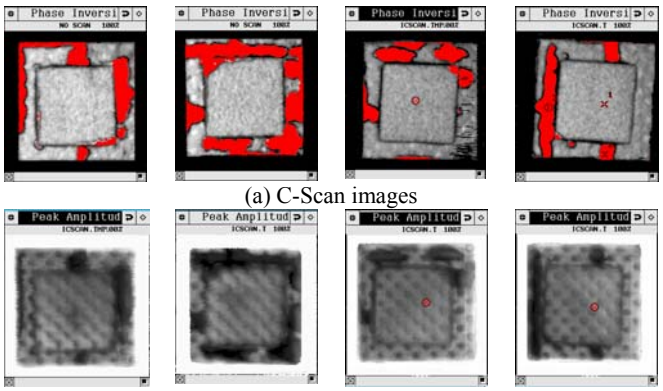

(a) C-Scan images

(b) T-Scan images

Figure 9. C-SAM Inspection of Package 2 after Test A

HYGRO-MECHANICAL STRESS ANALYSIS

In this study, the transient moisture diffusion and the subsequent hygro-mechanical stress modeling was performed using the coupled thermal stress analysis provided in the software. First the transient moisture field during reflow is derived then the swelling stress can be calculated with this moisture field. The governing equation of moisture diffusion is described by Fick's law as:

$$\frac{\partial C}{\partial t} = \alpha_m \left(\frac{\partial^2 C}{\partial x^2} + \frac{\partial^2 C}{\partial y^2} + \frac{\partial^2 C}{\partial z^2} \right) \tag{4}$$

where C is the moisture concentration, x, y, z are the spatial coordinates, α_m is the diffusivity and t is the time. However, the moisture concentration is not continuous at the interface. To

avoid this problem, wetness approach **[5]** is applied here as:

$$w = \frac{C}{C_{sat}}, \qquad 1 \geq w \geq 0 \tag{5}$$

where C_{sat} is the saturated moisture concentration, w is the wetness fraction. Here, w=0 means dry and w=1 means fully wet. Then Eq. (4) turns into:

$$\frac{\partial w}{\partial t} = \alpha_m \left(\frac{\partial^2 w}{\partial x^2} + \frac{\partial^2 w}{\partial y^2} + \frac{\partial^2 w}{\partial z^2} \right) \tag{6}$$

where $\alpha_m = D_m * C_{sat}$, D_m is the coefficient of moisture diffusion. Then Eq. (6) could be solved using a thermal element type in ANSYS code.

For moisture absorption modeling, the initial condition is w=0 for the whole package, and boundary condition is w=1 at the external surfaces which are exposed to the ambient moisture. Unfortunately, the moisture material properties are not usually provided from the material supplier due to the complex sample preparation and time consuming moisture diffusion testing. Therefore, the key parameter, moisture diffusion coefficient of molding compound, was measured in this study. According to ASTM standard **[6]**, a disk sample was fabricated under transfer molding process. A moisture weight gain was measured under 60°C and 60%RH (Accelerated MSL-3). Then the D_m and C_{sat} could be calculated according to these data in Figure 10.

For moisture desorption modeling, the Arrhenius equation is used to describe the diffusivity as a function of temperature.

$$D_m = D_0 e^{\frac{Q}{RT}} \tag{7}$$

where D_0 is the initial diffusion coefficient for moisture desorption, Q is the activation energy (ev), R is the Boltzmann constant (8.83e-5 eV/°K), and T is the absolute temperature (°K). Except for the D_m and C_{sat} of molding compound and die attach which are determined by experiments, other parameters for moisture analysis are from Reference **[1]**.

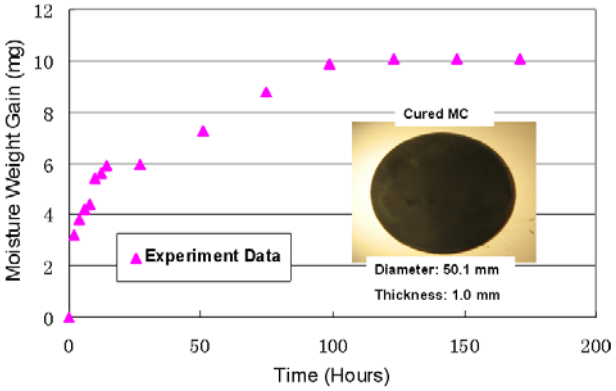

Figure 10. Moisture Absorption of Molding Compound under Accelerated MSL-3 Preconditioning

After calculation of Eq. (6), the moisture wetness distribution could be plotted in Figure 11. The package was fully wet after accelerated MSL-3 preconditioning. During the reflow, the moisture started to escape from the package. But, the time was insufficient for exclusion of all the moisture. Still a lot of moisture remained at the molding compound/lead-frame interface. Then the moisture could be considered for the calculation of coefficient of moisture expansion β (CME) induce stress as:

$$\varepsilon_M = \beta C = \beta C_{sat} \left(\frac{C}{C_{sat}} \right) = (\beta C_{sat}) w \tag{8}$$

where ε_M is the hygrostran, β is the CME. Solving Eq. (8), the hygro-mechanical stress acting in molding compound is plotted in Figure 12. The interfacial stress is also shown in Figure 13. Similar trend as the thermo-mechanical stress, the interfacial stress subjected to hygro-mechanical loading was dominated by shear stress. The highest value was achieved at point C.

Table 5. Material Properties for Moisture Analysis

	D_m (mm²/s)	C_{sat} (mg/mm³)	D_0 (mm²/s)	Q (eV)	β (mm³/mg)
MC	4.44e-6	5.1e-3	0.18	-0.31	0.22
DA	1.25e-5	3.2e-3	0.35	-0.29	0.52

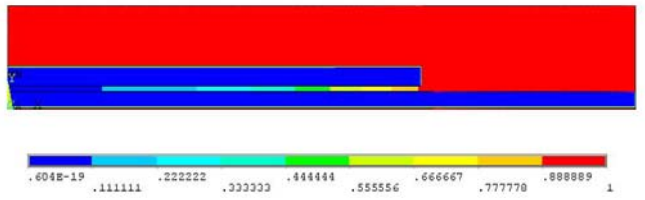

(a) Wetness distribution after preconditioning

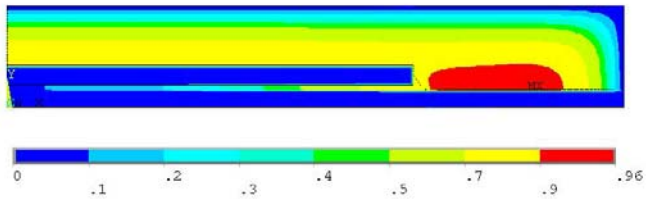

(b) Wetness distribution during reflow at 260°C

Figure 11. Moisture Absorption and Desorption

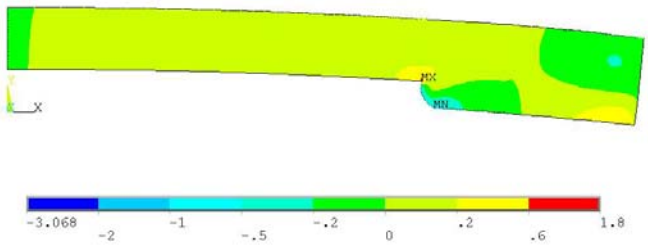

Figure 12. Shear Stress Acting in Molding Compound at 260°C under Hygro-mechanical Loading

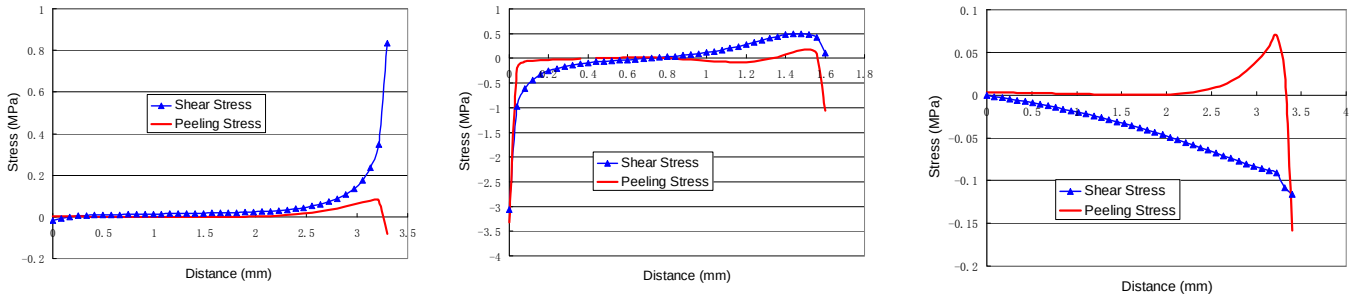

(a) Path 1, A-B (b) Path 2, C-D (c) Path 3, E-F

Figure 13. Interfacial Stress Distribution from Hygro-mechanical Stress Analysis at 260°C

INTEGRATED STRESS ANALYSIS

In MSL-3 test, the packages are subjected to hygrothermal effect during reflow. Both CTE and CME mismatch can induce the stress existing in the package. Therefore, an integrated stress analysis is required to represent the total package stress change during reflow. As mentioned earlier, Tee used an equivalent mean CTE method to consider both thermal and moisture effect together seen in Eqs. (9) and (10).

$$\left.\begin{aligned} \varepsilon_T &= \alpha_1 \Delta T \\ \varepsilon_M &= \beta C \Rightarrow \alpha_2 = \frac{\varepsilon_M}{\Delta T} \end{aligned}\right\} \Rightarrow \alpha_{total} = \alpha_1 + \alpha_2 \qquad (9)$$

$$\varepsilon_{total} = \alpha_{total} \Delta T \qquad (10)$$

α_1 is the original CTE, α_2 is the equivalent mean CTE transfer by moisture induced strain. Because the moisture induced strain is dependent on the moisture distribution. If the non-uniform moisture distribution is considered during reflow that means the different element will have different equivalent CTE. This disobeys the physics. Also, the hygro-mechanical stress is decreasing during reflow since the moisture is releasing. Once an equivalent CTE is used to represent the moisture induced strain, the moisture induced stress increase as the temperature increases. This disobeys the physics again. As a result, the equivalent mean CTE method assumes the moisture distribution is uniform during reflow. Also, the equivalent mean CTE model can not show the stress change during reflow correctly. It may be correct only at one point.

In this study, a superposition method is applied here to avoid the above issues seen in Eq. (11).

$$\left.\begin{aligned} \varepsilon_T &= \alpha_1 \Delta T \\ \varepsilon_M &= \beta C \end{aligned}\right\} \Rightarrow \varepsilon_{total} = \varepsilon_T + \varepsilon_M$$

(11)

The pure thermal stress analysis and hygro-stress analysis is running separately. Since they are all linear-elastic analyses, the thermo-mechanical stress and hygro-mechanical stress can be integrated directly by superposition. The major advantage of this approach is the hygro-mechanical stress analysis is conducted as a function of time and temperature by considering the moisture desorption during reflow. Figure 14 shows the stress change at Point C during reflow. It can be seen that the hygro-mechanical stress did not change much. This is because there is still serious local moisture concentration along the molding compound/lead-frame interface during reflow seen in Figure 11. Therefore, even though the hygro-mechanical stress is released, the integrated stress continues to increase with temperature increase and achieves the maximum value at peak temperature. Then, the integrated interfacial stress (Figure 15) along all three interfaces could be derived by integration of those values in Figures 6 and 13. The strength approach based on Eq. (3) could be applied to evaluate the MSL performance of dummy QFN again. The calculations of failure factors *D* were listed in Table 6. Some estimation is given as follows:

- The failure factors *D* calculated by integrated stress are lager than pure thermal effect. The value increase is about 22 %. Which means possibility to fail has been increased about 22% when the moisture effect is added.
- Compare the *D* in rows, the maximum value is located at point C, which means the delamination will initiate at molding compound/lead-frame interface around the junction of die attach fillet

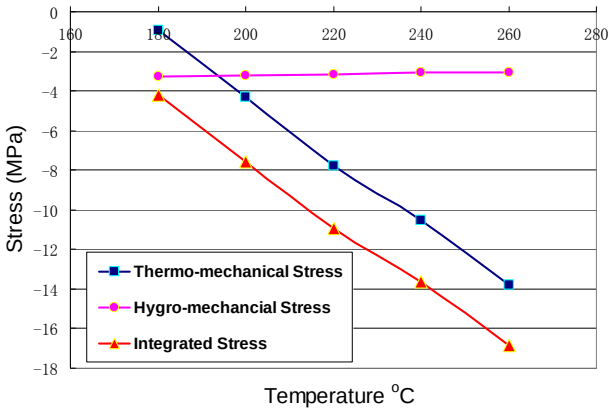

Figure 14. Stress Change during Reflow at Point C

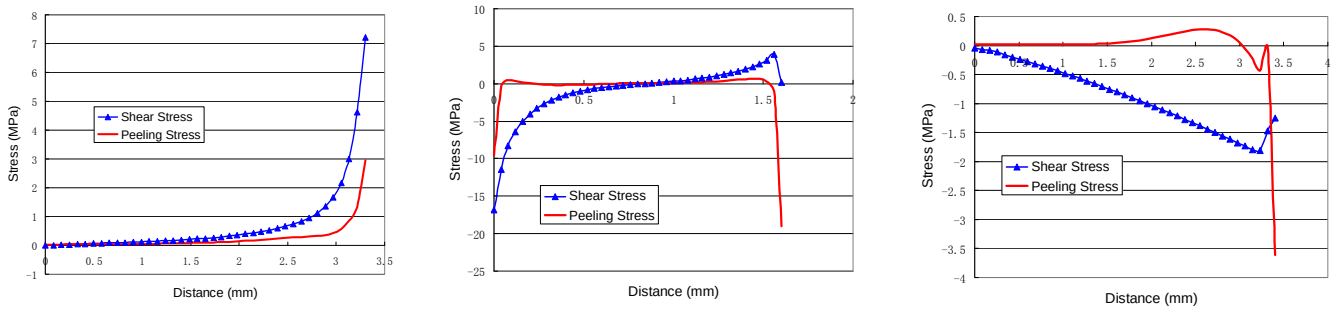

(a) Path 1, A-B (b) Path 2, C-D (c) Path 3, E-F

Figure 15. Integrated Interfacial Stress Distribution at 260°C

Table 6: Calculation of Integrated Failure Criterion Factors *D*

	1) MC/Si (A-B)		2) MC/LF (C-D)		3) DA/LF (E-F)	
	A	B	C	D	E	F
Maxi Shear Stress (MPa)	0	7.20	-16.87	3.92	0	-1.81
Maxi Peeling Stress (MPa)	0	2.94	-9.55	-18.98	0	-3.61
D_{Ag}=[τ/S]	0	0.72	**1.50**	0.35	0	0.24
D_{PPF}=[τ/S]	0	0.72	**2.23**	0.52	0	0.07

Now, the experiment validations were implemented following the test B in Figure 7. The dummy QFN went through reflow after 40 hours accelerated MSL-3 preconditioning following JEDEC standard **[7]**. The C-SAM inspections in Figures 16 and 17 showed that both package 1 and 2 failed at this time. Terrible delamination was found at molding compound/lead-frame and molding compound/Si(die top) interfaces. Focusing on the molding compound/lead-frame interface, most of the outside boundaries of the delam area pointing to the package edge were smaller than the inside ones. Considering the observations of the delamination propagation trend, most of the delamination was believed to be initiated at the junction of die attach fillet. This could be matched with the above estimation. Focusing on the molding compound/Si(die top), delamination were generated the edge of the die. This matched with the calculation of failure factors *D* along path 1 (A-B). Since point B had the higher value, it would be the initiation when delamination occurred at this interface.

Cross-sections of the failed sample after test B were photographed under Scanning Electronic Microscope (SEM). From the SEM images shown in Figure 18, the obvious crack tips have been observed. Both of them pointed to the die attach region, which proved that the delamination were initiated at MC/LF interface. Also, the thickness of the crack in package 2 is much thicker than that in package 1. This is reasonable because package 2 may already fail under the pure thermal effect. That reveals the delamination may be initiated earlier in package 2 and then the vapor pressure may take effect at a longer time on the delaminated surface. Therefore, the delamination opening could be larger in Package 2 due to the vapor pressure effect.

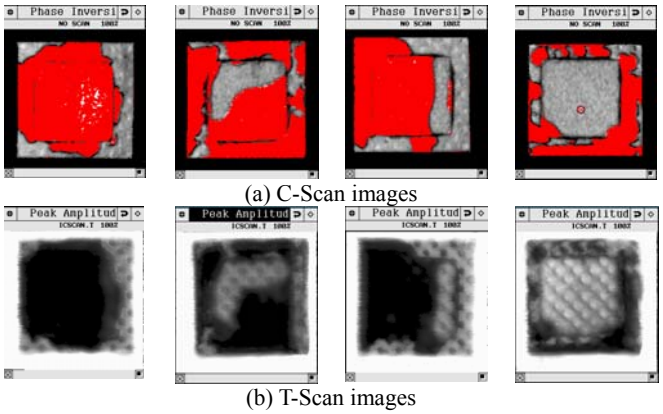

(a) C-Scan images

(b) T-Scan images

Figure 16. C-SAM Inspection of Package 1 after Test B

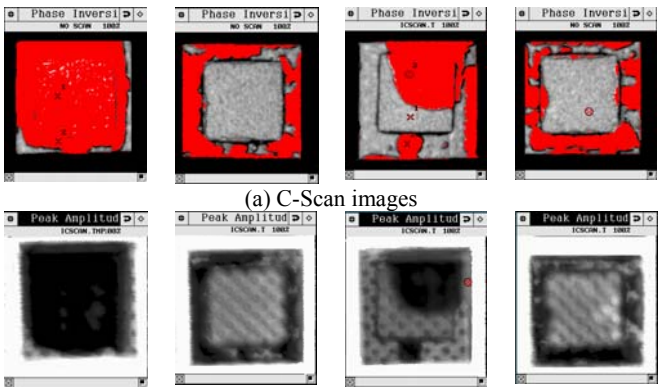

(a) C-Scan images

(b) T-Scan images

Figure 17. C-SAM Inspection of Package 2 after Test B

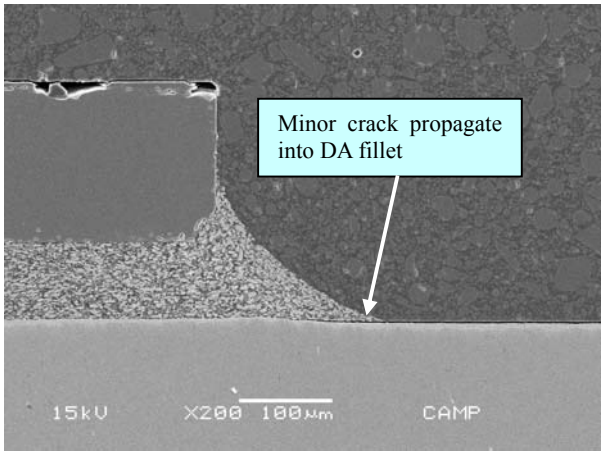

(a) Package 1 with Ag lead-frame

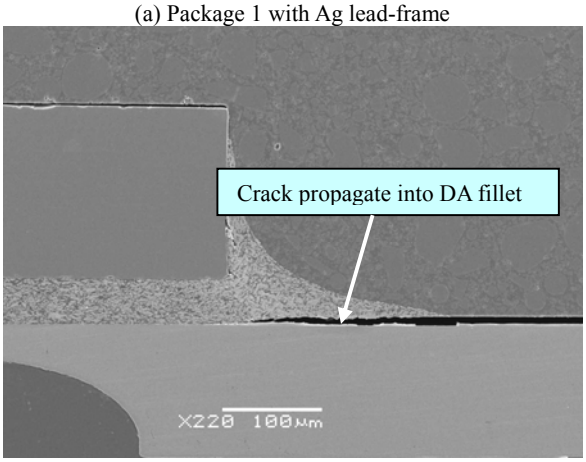

(b) Package 2 with PPF lead-frame

Figure 18. Cross-section Analysis of Dummy QFN after Test B

DISCUSSION

Fracture mechanics approach is another popular method to predict the delamination by comparing the stress intensity factor (K) or energy release rate (G) at different locations seen in references **[1]-[2]** and **[10]**. In order to derive the K or G, a pre-crack is embedded in the finite element model. However, the finite element model with an embedded pre-crack is different with the real situation where the sample is intact before reflow. Therefore, the fracture mechanics approach has some inborn defects to predict the delamination initiation. Also, the simulation results of fracture mechanics method are really dependent on the location and the length of the artificial pre-crack. Moreover, the complete discussion using fracture approach requires the interfacial fracture toughness. This is very difficult to determine by experiments due to the specific fabrication of electronic package interface. Therefore, to indicate the initiation of delamination, strength approach has more advantages compared to fracture mechanics approach such as simple modeling techniques without pre-crack effects and available experimental measurements of interfacial strength.

However, the major issue using strength approach is that the stress value is mesh-dependent. In this paper, the stress ratio D is not treated as an accurate failure criteria. Normally when $D>1$ means the failure happened. But here, the comparison of D was implemented in the relative way. Therefore, the estimation by the strength approach is not mesh-dependent. Compared to the stress singularity, two more critical issues that affect the calculation of D should be mentioned here. First issue is the stress calculated from FEA is all above 175°C. But the interfacial strength used here is all determined at room temperature due to experiment limitations. This may induce some underestimates for D since the interfacial strength will decrease with temperature increasing. Therefore, the interfacial adhesion test at high temperature is scheduled in the future work. The other issue is both thermo-mechanical and hygro-mechanical models use the linear-elastic material properties. This would be different with the real situation in that the electronic materials will behave in a thermal-plastic way at high temperature. This may induce some overestimates for D. Even with some inaccurate problems in calculation of D, the strength approach still works since it agrees well with the experiment results.

Vapor pressure is another key factor which will affect the moisture related failure. Many papers have discussed the applications of vapor pressure calculations **[8]-[9]**. However, there are some issues with the vapor pressure calculations at high temperature. Therefore, we assume the major contribution of vapor pressure is to induce the crack propagation. In this study, the main concern is focused on the delamination initiation.

CONCLUDING REMARKS

In general, a complex system was established to evaluate the package reliability against delamination. Both simulation and experiment validations have been implemented to study the failure mechanism of interfacial delamination. From the comparison between FEA and experiments, conclusions could be given as follows:

1. Two types of dummy QFN packages have been fabricated as the test vehicle of the subsequent study. Experiment tests with pure thermal effect and with hygrothermal effect on the dummy packages were conducted. Detailed inspection of delamination was performed to characterize the failure modes.
2. A finite element model for dummy QFN package has been built up to run the stress analysis when package is subjected to pure thermal loading and hygrothermal loading. For both analyses, the shear stress was found to be the dominant stress component. The maximum stress value appeared at MC/LF interface around the junction of die attach fillet.
3. A superposition method was developed to integrate the thermo-mechanical and hygro-mechanical stress together by considering the non-uniform moisture distribution

during reflow. Since the local moisture concentration did no change much along the interfaces, the hygro-mechanical stress change was not obvious. As a result, the integrated stress change with temperature was similar to the thermo-mechanical stress change.

4. Based on the result of stress calculations, strength approach was applied here to evaluate package reliability and to indicate the delamination initiation. The analyses of strength approach agreed well with the experiment results. Package 1 with Ag lead-frame has better reliability against delamination than package 2. Also, the delamination is believed to be initiated at the molding compound/lead-frame interface around the junction of die attach fillet in dummy QFN.

REFERENCES

[1] T.Y. Tee and Z.W. Zhong, "Integrated vapor pressure, Hygroswelling, and thermo-mechanical stress modeling of QFN package during reflow with interfacial fracture mechanics analysis," *Microelectronics Reliability*, Vol. 44 2004, pp 105-114.

[2] W.D. Driel *et al*., "Driving Mechanisms of Delamination related Reliability Problems in Exposed Pad Packages," *IEEE Transactions on Components and Packaging Technologies*, 2007, pp 223-229.

[3] M.S. Zhang and R.S.W. Lee, "Investigation of Moisture Sensitivity Related Failure Mechanism of Quad Flat No-lead (QFN) Packages," *ASME IMECE.,* Boston, Massachusetts, 1-6 November, 2008. (IMECE2008-68120)

[4] J.H. Lau, "A Note on the Calculation of Thermal Stresses in Electronic Packaging by Finite Element Methods," *Journal of Electronic Packaging,* Vol. 111, Dec 1989, pp 313-320.

[5] E.H. Wong, Y.C. Teo and T.B. Lim, "Moisture Diffusion and Vapor Pressure Modeling of IC Packaging," *Proc.48th Electron. Comp. Technol. Conf.*, 1998, pp. 1372-1378.

[6] "Standard Test Method for Water Absorption of Plastics," 1998. ASTM D570

[7] IPC/JEDEC J-STD-020D, "Moisture/Reflow Sensitivity Classification for Nonhermetic Solid State Surface Mount Devices", *JEDEC Solid State Tech. Assoc 2007*

[8] X.J. Fan *et al*., "A Micromechanics-Based Vapor Pressure in Electronic Packages," *Journal of Electronic Packaging,* Vol. 127, Sep 2005, pp 262-267.

[9] J.H. Lau and S.W.R. Lee, "Temperature-Dependent Popcorning Analysis of Plastic Ball Grid Array Package during Solder Reflow with Fracture Mechanics Method," *Journal of Electronic Packaging,* Vol. 122, No. 1, Mar 2005, pp 34-41.

[10] A.A.O. Tay, "Modeling of Interfacial Delamination in Plastic IC Packages under Hygrothermal Loading," *Journal of Electronic Packaging*, Vol. 127, Sep 2005, pp 268-275.